

Punching Shear Performance of High-compressive Flat Slabs Reinforced with Hybrid Fibres

Mohammed S. Al Jawahery^{1*}, Rayan Faiz Hadi Boto², Mehmet Tolga Göğüş²

¹ Civil Engineering Department, College of Engineering, University of Mosul, Al Majmoaa Street, 41002 Mosul, Iraq

² Civil Engineering Department, Gaziantep University, Üniversite Bulvarı, 27310 Gaziantep, Türkiye

* Corresponding author, e-mail: mohammed.aljawahery@uomosul.edu.iq

Received: 23 June 2024, Accepted: 04 March 2025, Published online: 26 March 2025

Abstract

A framework is presented to explore the influential role of hybrid fibers on the performance of two-way flat slabs against punching shear failure. A finite element (FE) modeling approach *via* the ATENA-GiD software package is used to simulate the case study. Four variables are covered in this investigation including different mix proportions of hybrid fiber-reinforced concrete (HFRC), which contains 0.2% of macro synthetic fibers, and (0.68, 0.8, and 0.96%) steel fibers (SFs) (volumetric ratios), high compressive strengths of 50, 70, and 90 MPa, different main steel reinforcement ratios based on main steel bars of 16, 20, and 25 mm, as well as 150, 200, and 250 mm as thicknesses of the slab. 106 two-way slabs (1900 × 1900 mm) models were generated in this investigation, besides 8 verification materials models. Furthermore, a parametric analysis was performed on the results of FE modeling. The FE modeling results of verification materials tend to be accurate with a correlation coefficient ($R^2 = 0.9578$). Moreover, the outcomes of the study show; that the hybrid fibers' effective ratio comprises about 0.96% SFs and 0.2% macrosynthetic fibers, using 0.54% of main steel reinforcement ratio which is supposedly more economical than other ratios of main reinforcement, 150 mm is a crucial thickness of the flat slab with 70 or 90 MPa as high compressive strength. The combined results can enhance the performance of the flat slab by preventing shear punching failure.

Keywords

nonlinear FE analysis, ATENA-GiD programs, flat slab, hybrid fiber-reinforced concrete (HFRC), high compressive strength, punching shear failure

1 Introduction

In any multi-story building, the slabs serve as the primary structural elements that directly support the live load. When a slab is flat, it means that it rests directly on columns without beams. Consequently, the depth of the flat slab is primarily influenced by the resisting shear stresses near the columns [1–4]. To minimize the thickness of the slab and prevent catastrophic column failure, the designer must either reduce the shear stress at the edge between the slab and column or increase the shear resistance in this area [5–7].

Fiber-reinforced concrete (FRC) enhances structural integrity and longevity by integrating diverse fiber materials. This blend mitigates cracking triggered by concrete's plasticity and drying shrinkage. Common fibers like polypropylene, glass, and steel are integrated into the mix. Hybrid fiber-reinforced concrete (HFRC), on the other hand, combines two or more fiber types for superior performance [8–10]. The choice to combine two types of

fibers may stem from their distinct properties or cost-related factors. The combination of steel and polypropylene fibers (PPFs) led to a significant improvement in load-deflection behavior [11, 12]. Steel fibers (SFs) are small pieces of steel with a length-to-diameter ratio of 20 to 100 (aspect ratio). Their cross-sections vary, and their small size allows for even mixing into regular concrete without the need for curing. Synthetic fibers are a kind of fiber product from petrochemical and textile industry research and development [13, 14]. Conversely, synthetic fibers are integral in the initial phases of composite materials, particularly when the matrix is fragile, brittle, and possesses a low modulus. Moreover, in fully developed concrete, enhancing material durability relies on both the volume of fibers and the matrix's strength. The effectiveness of the fiber-matrix bond depends on the fiber surface area, which increases with a higher surface-to-volume ratio. Therefore, fibers

with a rectangular cross-section are better than round fibers. In addition, fibers with greater length and smaller diameter (higher aspect ratio) are more effective [15, 16].

Punching shear failure is a type of brittle failure that happens due to the application of a concentrated force supplied to a slab [17, 18]. The punching shear strength of flat slabs is subject to numerous factors, among which the compressive strength of the concrete (f'_c) stands out as particularly significant. This influence becomes apparent either directly or indirectly, especially when considering the tensile strength of the concrete (f_t). Another crucial factor is the geometric ratio of the longitudinal reinforcement. Moreover, the depth (d) of the slab, rather than the thickness of slab (h), holds significance. Increased depth augments both the punching shear strength and the flexural strength of the slab [6, 19]. Deficits in tensile strength, stiffness, flexural strength, shear strength, and brittleness within the material can lead to punching defects in concrete [20]. Still, punching shear failure remains one of the most frequent failure modes for this structural system. It occurs suddenly and unexpectedly, resulting in catastrophic consequences [21].

The following several selected brief studies give the researchers more knowledge about the efficient role of mixing several types of fibers in a matrix of composite materials. Abbass et al. [22] examined how the inclusion of SFs of various lengths and diameters affected the mechanical properties of concrete across three different strength grades. Using hooked-ended fibers of lengths 40, 50, and 60 mm, and diameters 0.62 and 0.75 mm, alongside three water-to-cement ratios (0.25, 0.35, and 0.45), the experiment explored the impact of SFs at volume fractions of 0.5%, 1.0%, and 1.5%. Thirty concrete mixes were prepared and tested. The results showed that altering the fiber content and length, alongside adjusting the water-to-cement ratio, significantly influenced concrete's mechanical properties. Notably, there was an increase in compressive strength by 10–25% and in indirect tensile strength by 31–47% with SF additions from 0.5% to 1.5%. Moreover, flexural strength rose by 3% to 124% with fibers of aspect ratio < 65 , and by about 140% with an aspect ratio of 80, compared to concrete without fibers. Tan and Venkateshwaran [23] explored the effect of SFs on the punching shear behavior of slabs without any steel bar reinforcement by casting twelve square slabs. The parameters that were covered in this study were different multi-hook end types of SFs, compressive strength, slab thickness as well as the index of reinforcing. The yield

line theory was used to assess the load capacity of slabs. The study's authors observed that the yield line theory accurately predicts the load capacity of experimental samples. Moreover, all-SF slabs failed in flexural mode rather than punching shear failure because the energy that was required to propagate cracks to fail in flexure was less than to fail in punching shear, which needed more energy to create the circumferential cracks around the column face.

Labib [8] published a research article that is focused on the behavior of hybrid steel-PPFs to improve the punching shear resistance of the concrete slab connection. This study includes three mixtures besides the reference plain concrete mixture, fiber type and volume mix were factors that have been entered in mixtures. A significant improvement was observed in the punching shear capacity when using hybrid fiber concrete mixes rather than a single type of fiber concrete mixes. Moreover, the mixture which has 0.2% of polypropylene fiber and 1.5% of SF in a volumetric ratio, gives a notable increase of 34% in punching shear capacity.

AlHamaydeh and Anwar Orabi [24] examined the effectiveness of synthetic fiber reinforcement in enhancing the shear capacity of flat slabs reinforced with glass fiber-reinforced polymer bars. The experimental setup involved six large-scale slabs. Their findings revealed that the addition of synthetic fibers led to a slight improvement in punching shear resistance compared to the control slabs, with an average increase in toughness by a factor of 2.34.

Khan et al. [25] studied the behavior of twenty-one simply supported two-way slabs experimentally and finite element (FE) modeling. Slabs were produced with a selected volumetric proportion of hybrid fibers (SF) from 0.7 to 1.0% with PPFs from 0.1 to 0.9%). The slabs were tested under flexural loading. Moreover, the results show that the ideal proportion of 0.9% SF combined with 0.1% PPF gave a significant carrying load capacity, ductility, as well as cracks. The FE model showed a close agreement with the experimental results.

This study seeks to examine the impact of achieving an optimal hybrid fiber ratio (combining SFs with macro-synthetic fibers) to enhance performance against punching shear failure in flat slabs. This will be accomplished through FE modeling to simulate a new case study. The study incorporates various variables, including the HFRC mix proportion, high compressive strength, longitudinal reinforcement ratio, and slab thickness. Additionally, parametric analysis will be conducted to elucidate the individual roles of each parameter in this investigation.

2 Methodology

2.1 Characterization of experimental data

The initial phase of the study involves validating the materials used in FE modeling, including concrete, steel reinforcement, fibers, and the load-bearing plate applied to the test slabs, by comparing them with selected experimental studies from the literature. The level of validation directly influences the accuracy of the FE results. Eight test slabs were chosen from the literature for this validation process [21].

The study comprises two groups, each containing four slabs. In each group, one slab serves as a reference (*R*), while the other slabs feature varying volumetric ratios of HFRC. The slabs measure 1900×1900 mm in length and width, with thicknesses of 200 mm for the first group and 250 mm for the second group. The slabs were centrally loaded using a 250×250 mm column stub with simply supported conditions along all four sides. The volumetric ratios of fibers for both groups were 0, 0.68, 0.8, and 0.96% for SFs and 0.2% for macro-synthetic fiber. Fig. 1 illustrates the dimensions and reinforcement details of a typical test slab. All test slabs used 25 mm steel reinforcement, and the spacing was determined as reported in Table 1 [21].

The SFs utilized were of the hooked-type design, whereas the synthetic fibers had a 90-aspect ratio. Table 2 outlines the manufacturer's specifications for the fibers employed in this investigation. Table 3 details the compressive and flexural tensile strengths of all HFRC mixtures used in the slabs.

2.2 Illustrate of nonlinear FE analysis

The nonlinear FE analysis was conducted using the ATENA-GiD software packages [26]. Data preparation and mesh creation for the models were performed using GiD, while the FE analysis itself was executed using the ATENA software [26]. ATENA, developed by Cervenka Consulting, is a nonlinear FE program specifically designed for the analysis of reinforced concrete structures [27]. The nonlinear FE models comprise a total of 108 instances, categorized into three groups. Each group shares the same shape and dimensions as the experimental verification samples. Each group has thirty-six models within the main variables based on: concrete compressive strength (f'_c) of 50, 70, and 90 MPa, slab thickness (h) of 150, 200, and 250 mm, hybrid fiber volume ratio (VF (%)) which consists of two types: the first one the SF within three volumes of 0.68%, 0.8%, and 0.96% besides mix with the macro synthetic fibers constitute about 0.2% of the volume of the sample, and main steel reinforcements were explored by using three quantities of reinforcement in the main layer of samples. The steel bar diameters in the bottom layer were 16 mm, 20 mm, and 25 mm, with corresponding reinforcement ratios (A_s/A_c) of 0.54%, 0.84%, and 1.31%, respectively, for slabs of 150 mm thickness; 0.4%, 0.63%, and 0.98% for 200 mm thickness; and 0.32%, 0.5%, and 0.79% for 250 mm thickness. Additionally, 10 mm diameter steel bars were employed for reinforcement in the top layer of all modeled slabs, with a spacing

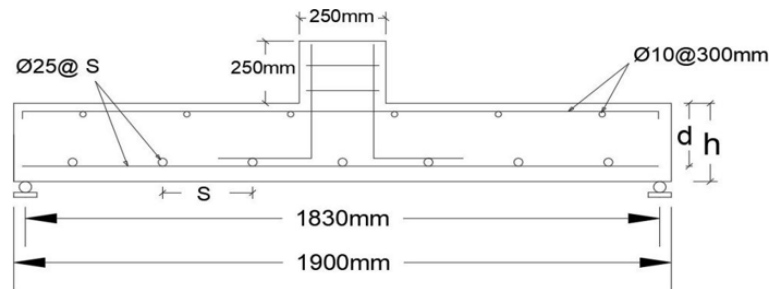


Fig. 1 Details of a test specimen [21]

Table 1 Slabs property detail [21]

No.	Groups	Specimen	d (mm)	V_f steel (%)	V_f synthetic (%)	Reinforcement	Bar spacing (mm)
1	200 mm thickness of the slab	R 200	145	0	0	7#25	265
2		HFR200-0.68/0.2	145	0.68	0.2	7#25	265
3		HFR200-0.80/0.2	145	0.80	0.2	7#25	265
4		HFR200-0.96/0.2	145	0.96	0.2	7#25	265
5	250 mm thickness of the slab	R 250	195	0	0	9#25	195
6		HFR250-0.68/0.2	195	0.68	0.2	9#25	195
7		HFR250-0.80/0.2	195	0.80	0.2	9#25	195
8		HFR250-0.96/0.2	195	0.96	0.2	9#25	195

Table 2 Fiber properties as provided by manufacturer [21]

	Fiber type	Symbol and value	Hooked
SFs	Fiber length	L_f (mm)	50
	Fiber diameter	D_f (mm)	1.1
	Ultimate tensile strength	MPa	1100
Macro synthetic fibers	Fiber length	L_f (mm)	40
	Fiber diameter	D_f (mm)	0.45
	Ultimate tensile strength	MPa	620

Table 3 Compressive strength and modulus of rupture of different mixtures [21]

No.	Concrete mixtures	V_f steel (%)	V_f synthetic (%)	Concrete strength f'_c (MPa)	Modulus of rupture (f_r) (MPa)
1	Reference	0	0	70	5.45
2	HFRC-0.68	0.68	0.2	77	7.10
3	HFRC-0.80	0.80	0.2	61	7.20
4	HFRC-0.96	0.96	0.2	60	8.35

Table 4 All parameters which are included in the parametric analysis

Slab thickness (h) (mm)	f'_c (MPa)	Reinforcement ratio (ρ) (%)	SFs (%)				Macro synthetic fibers (%)
150	50	0.54	0	0.68	0.8	0.96	0.2
		0.84					
		1.31					
		0.54					
		0.84					
		1.31					
	70	0.54	0	0.68	0.8	0.96	0.2
		0.84					
		1.31					
		0.54					
		0.84					
		1.31					
200	50	0.4	0	0.68	0.8	0.96	0.2
		0.63					
		0.98					
		0.4					
		0.63					
		0.98					
	70	0.4	0	0.68	0.8	0.96	0.2
		0.63					
		0.98					
		0.4					
		0.63					
		0.98					
250	50	0.32	0	0.68	0.8	0.96	0.2
		0.5					
		0.79					
		0.32					
		0.5					
		0.79					
	70	0.32	0	0.68	0.8	0.96	0.2
		0.5					
		0.79					
		0.32					
		0.5					
		0.79					

of 300 mm c/c. Table 4 provides a comprehensive overview of all parameters considered in the modeling for this study.

2.3 Constitutive models for nonlinear FE analysis

In this study, the Fracture-Plastic model was employed to merge constitutive models for tensile (fracturing) and compressive (plastic) behavior. The fracture model is grounded in the orthotropic smeared crack formulation and the crack band concept. It encompasses the Rankine failure criterion, exponential softening, and can function as either a rotating or fixed crack model. The hardening/softening plasticity system is based on the Menétrey-Willam failure surface, integrating constitutive equations through a return mapping technique. This model accommodates concrete cracking, crushing under high confinement, and fracture closure, allowing for the simulation of crushing in other material directions [28, 29]. Fig. 2 illustrates the 3D failure surface model.

The steel reinforcement is modeled using the elastic-perfectly plastic model with a bilinear law. The initial section of Fig. 3 represents the elastic behavior with the steel's elastic modulus (E_c). The subsequent line signifies the onset of plasticity in the steel, featuring hardening with a slope represented by the hardening modulus E_{sh} . In cases of perfect plasticity, E_{sh} equals 0. The limit strain ε_L denotes the restricted ductility of the steel. Fig. 3 illustrates the bilinear law applied to the reinforcement [29].

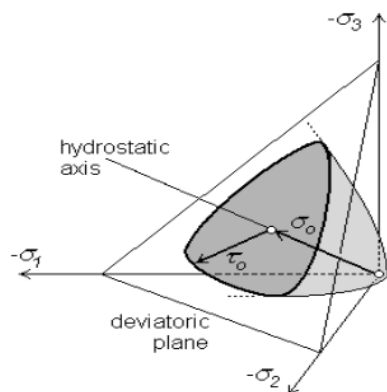


Fig. 2 Menétrey-Willam model of 3D failure surface [28, 29]

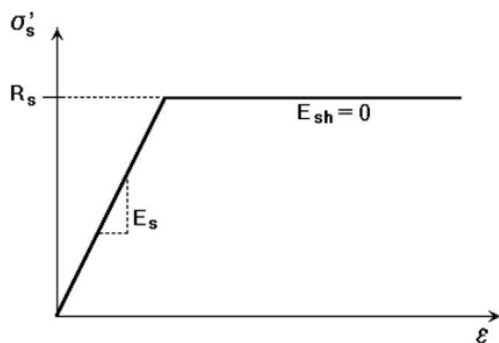


Fig. 3 FE The bilinear stress-strain law for reinforcement [29]

Embedded reinforcement elements that were used to model the steel reinforcement. The smeared concept assumes a perfect bond between concrete and reinforcement, meaning that direct modeling of bond slip is not possible, except for the inherent effects of tension stiffening. However, at the macro level, a relative slip displacement between the reinforcement and the surrounding concrete can occur over a certain distance if the concrete is cracked or crushed. This represents the actual mechanism of bond failure observed in ribbed bars.

It can be concluded that the analysis is based on a commonly used embedded reinforcement interaction model that assumes a perfect bond between the concrete and the reinforcement. This technique is in line with the smeared reinforcement approach, as defined in the ATENA Program Documentation ([29]:p.17), which does not explicitly model bond-slip but introduces its influence through additional mechanisms. In other words, the bond is assumed to be perfect at the level of micro constituents, meaning no relative slip occurs between the reinforcement and the concrete.

Nevertheless, the CEB-FIB Model Code 1990 ([29]:p.69), establishes a general definition of the mean bond strength-slip relationship that is used indirectly in this analysis. On a larger scale, if the surrounding concrete is cracked or crushed, there can be relative slip displacement between the reinforcement and surrounding concrete, representing the actual mechanism of bond failure for ribbed bars.

Additionally, regarding Fig. 4 and Table 5 ([29]:pp.70–71), the parameter of the initial slip threshold (S_1), which is the primary slip threshold, is considered to be 1 mm. This value is quite small and can be ignored for this analysis, as the study focuses only on ultimate load and ultimate displacement in the elastic zone, rather than the plastic zone. This assumption aligns with reality because bond-slip effects are negligible under service load conditions

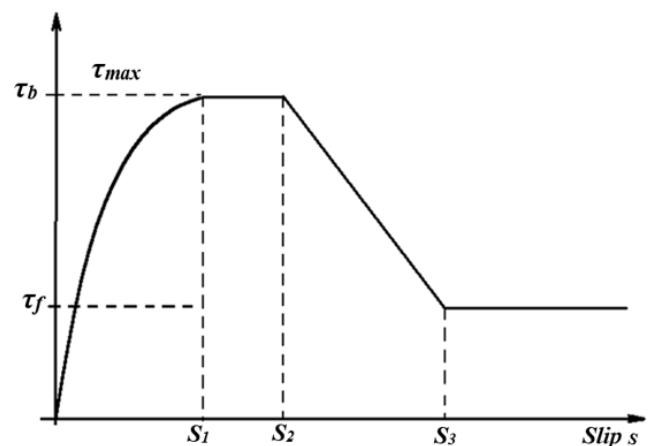


Fig. 4 Bond-slip law by CEB-FIP Model Code 1990 [29]

Table 5 Parameters for defining the mean bond strength-slip relationship for ribbed bars [29]

	2		3		4		5	
Value	Unconfined concrete*				Confined concrete**			
	Bond conditions		Bond conditions		Bond conditions		Bond conditions	
	Good	All other cases	Good	All other cases	Good	All other cases	Good	All other cases
S_1	0.6 mm	0.6 mm					1.0 mm	
S_2	0.6 mm	0.6 mm					3.0 mm	
S_3	1.0 mm	2.5 mm			Clear rib spacing			
α		0.4					0.4	
τ_{\max}	$2.0\sqrt{f_c}$	$1.0\sqrt{f_c}$			$2.5\sqrt{f_c}$		$1.25\sqrt{f_c}$	
τ_f		$0.15 \tau_{\max}$					$0.40 \tau_{\max}$	

* Failure by splitting of the concrete

** Failure by shearing of the concrete between the ribs

(i.e., typically 40% to 70% of the steel's yield point) and do not significantly affect the elastic behavior of the structure.

Therefore, it is reasonable to apply a smeared reinforcement model with a perfect bond assumption in this context, and the effects of bond-slip, as inherent to the CEB-FIB Model Code 1990 [29], are sufficiently covered within this framework. This corresponds with the focus on elastic behavior under service and ultimate loading conditions.

The present work specifically does not apply a bond-slip model in the numerical analysis. Rather, it made use of the embedded reinforcement technique offered by ATENA-Gid software [26], which by default presumes a full bond interaction. The following guided the choice of this method:

1. Behavior under service loads: regarding service-level criteria, the slip at the interface between reinforcement-concrete is insignificant. Usually reaching only roughly 70% of the reinforcement's yield strength, the loads in this work fall within a range where the bond mechanisms stay intact. This guarantees efficient force transfer without appreciable slip, hence the complete bond assumption is a useful and correct approximation for the structural behavior under service loads.
2. Conformity with research aims: this study primarily concentrated on the global response of the structure under service and ultimate loads, namely within the elastic range, rather than on intricate local phenomena such bond-slip interactions. Consequently, the comprehensive bond assumption effectively encompasses the essential elements of structural performance pertinent to the study's aims.
3. Modeling simplicity and efficiency: incorporating a detailed bond slip model would increase the computational complexity of the analysis, which was unnecessary given the study's emphasis on elastic behavior and ultimate load capacity. The ATENA Program

Documentation ([29]:p.71) talks about the CEB-FIB Model Code 1990 [29]. This code indirectly takes into account bond-slip effects at the macro level by using parameters like S_1 , which in this case is 1 mm. This value is small and negligible compared to the elastic behavior considered in this analysis.

Although an explicit bond-slip model was not employed in this work, it recognizes the significance of research focused on ultimate limit states, localized cracking, or other phenomena where bond-slip effects are crucial. Future research may investigate the incorporation of these models to enhance the analysis in scenarios when bond-slip behavior substantially affects structural performance.

The consideration of a bond-slip model could indeed help reduce the differences between experimentally measured displacements and those obtained from numerical simulations. Bond-slip behavior affects the local interaction between reinforcement and the surrounding concrete, particularly in scenarios where relative displacement at the interface influences the overall structural response. This becomes especially relevant with reduced span sizes and larger reinforcement diameters, such as the 25 mm bars used in this study, as these factors can amplify stress concentrations and bond-slip effects under high loads.

In the current study utilized the embedded reinforcement method provided by ATENA-GiD software [26], which assumes a perfect bond between concrete and reinforcement. This approach does not explicitly model bond-slip but indirectly accounts for its effects through mechanisms such as tension stiffening and the macro-level representation of cracked concrete behavior. This choice was made based on the following considerations:

1. Focus on global behavior: the study prioritized overall structural behavior over localized phenomena, considering bond-slip effects secondary to its objectives.
2. Displacement differences: observed discrepancies in displacements may stem from the absence of explicit bond-slip modeling, which could better align numerical results with experiments, especially near cracking or yielding.
3. Modeling simplicity: to maintain computational efficiency, the study used indirect methods (e.g., parameters from the CEB-FIB Model Code 1990 [29]) rather than implementing a detailed bond-slip model.
4. Future opportunities: incorporating a bond-slip model in future work could enhance simulation accuracy for localized effects and ultimate limit states.

In conclusion, while bond-slip modeling was outside the study's scope, its inclusion in future analyses is recommended to improve the representation of reinforcement-concrete interaction.

In the constitutive crack opening model, as depicted by the piecewise linear relations in Fig. 5, crack-normal stress components are correlated with cracking strains, representing the opening of multiple localized cracks. Multiple cracks are considered to remain open unless subjected to crack-normal compression (similar to plasticity-like unloading), while a localized crack is assumed to gradually close until the normal stress reduces linearly to zero top of form [29].

The constitutive model used for SFs embedded within the concrete material employed a specialized material model known as "Cementitious2 User (FRC)", available in the Atena-Guide software [27]. Cementitious2 User (FRC) is designed specifically for strain-hardening cementitious composites featuring randomly oriented fibers made from various materials such as steel, polymers, glass, etc., applied in different fractions. This model accounts for FRC specifications, including the shape of the tensile softening branch, high toughness, and ductility, to accurately simulate FRC behaviors. For guidance on defining user material response functions and detailed descriptions of models for tensile (fracturing) and compressive (plastic) behavior, refer to the ATENA Manuals [27, 30]. All information regarding the values of different types of concrete properties with the ratio of hybrid SFs is listed in Appendix A. The geometry of the concrete model is 3D solid hexahedron (brick) components with 8 nodes (CCIsoBrick<xxxxxxx>). The steel reinforcing bars were modeled using 3D truss elements with 3 nodes (CCIsoTruss<xxx>), it can be used to define the material parameters for bars or tendons based on the reinforcement steel strength class, with a few basic parameters (E_c , characteristic, yield strength, ...) and safety format. The loading plate and supports were modeled using 3D solid tetrahedral components with four nodes (CCIsoTetra<xxxx>), which is a linear elastic isotropic

material for 3D. At last, contact between two surfaces was modeled using pentahedron interface components with 12 nodes (CCIsoGao<xxxxxxxxxxx>) [27, 29].

2.4 Slab FE model

The Atena-GiD interface software program [26] was employed to simulate the slabs, each measuring 1900×1900 mm with varying thicknesses of 150, 200, and 250 mm. To exploit symmetry in the slab specimens and expedite the analysis process, only a quarter of the test specimens were simulated. All boundary conditions of the test slabs were assumed to accurately represent the real conditions observed in the laboratory. Figs. 6 and 7 depict the boundary conditions of the test slab and the mesh generation for the FE analysis, respectively.

3 Description and discussion of results

3.1 Verification results of HFRC slabs via FE modeling

One crucial aspect of FE modeling is validating the experimental materials of the specimens. To achieve this, experimental results were compared with the data from FE analysis models, encompassing four slabs of 200 mm thickness and four slabs of 250 mm thickness, each with varying ratios of hybrid SF. From the total number of specimens, two slabs were designated as reference slabs for both thicknesses. Table 6 presents the ultimate load capacities and deflections of the experimental and FE modeling results for HFRC slabs with thicknesses of 200 mm and 250 mm.

A statistical evaluation between the results of test slabs and FE modeling results (as shown in Fig. 8) was performed to demonstrate the degree of matching between them. Moreover, it can be observed from Fig. 7 that the correlation coefficient $R^2 = 0.9578$ indicates good compatibility between the FE modeling analysis, and test slabs, as well as the accuracy of FE modeling analysis by using ATENA-guide software [27] reliability to do more analysis.

Figs. 9 to 12 show the load-deflection curves of test HFRC slabs and FE modeling, analysis for both 200 and 250 mm thickness groups. These curves suggest that the ultimate loads predicted by the FE modeling align well with the results obtained from the test slabs. However, a significant disparity in stiffness is observed between the curves of the test and FE modeling slabs. This variation can be attributed to the assumptions made in the FE modeling process. A perfect connection between steel reinforcement and concrete is one of these hypotheses while in reality slipping may occur between them, which leads to the differences in the stiffness between the modeling and test results [31–35].

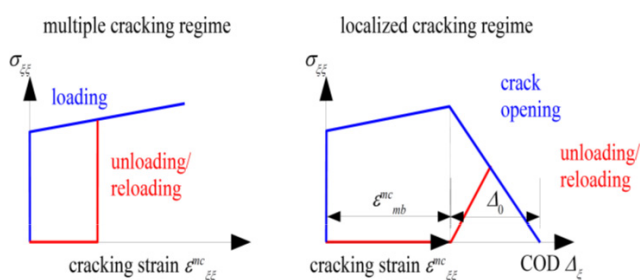


Fig. 5 Crack-normal direction in stress vs. cracking strain relations [29]

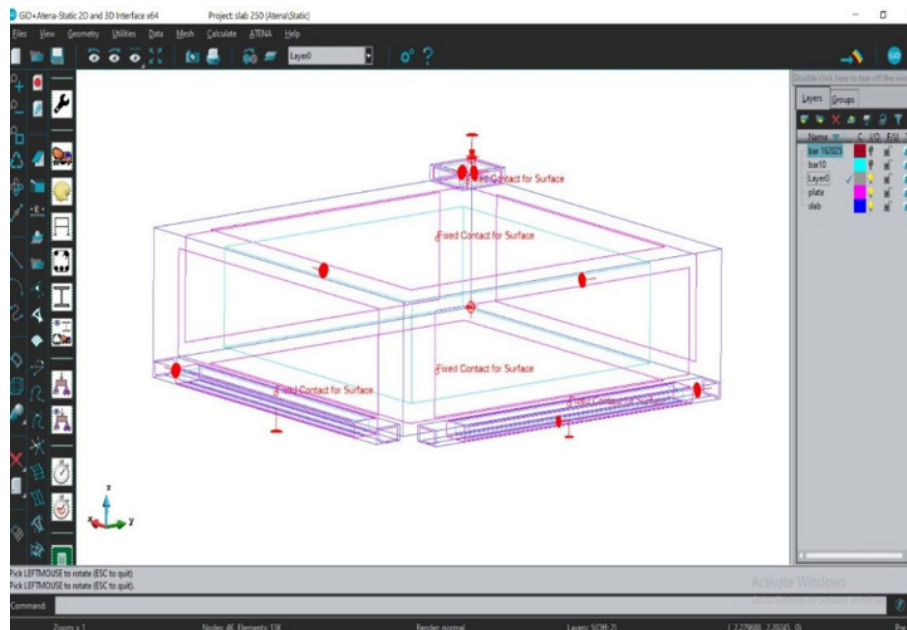


Fig. 6 Displays supports, boundary conditions, loads, and monitors point

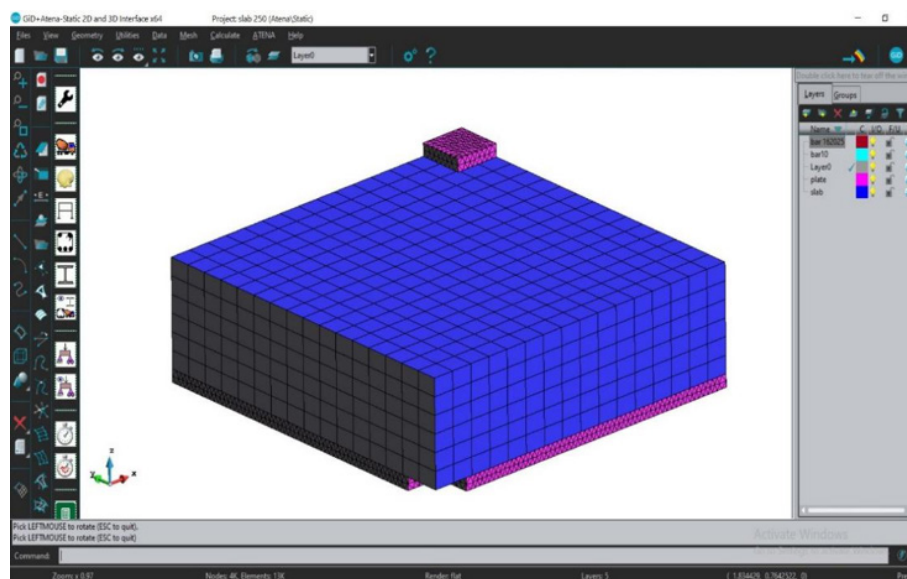


Fig. 7 Displays the generation of FE mesh in HFRC slab

Table 6 The ultimate load and deflection values for both experimental and FE models of HFRC slabs with thicknesses of 200 mm and 250 mm

No.	Specimens name	Experimental		FE	
		$P_{exp.}$ (kN)	$\Delta_{exp.}$ (mm)	P_{ATENA} (kN)	Δ_{ATENA} (mm)
1	R 200	847.9	19.91	863.15	10.65
2	HFR200-0.68/0.2	978.1	21.23	1008.69	11.2
3	HFR200-0.80/0.2	1029.9	16.97	1014.63	14.95
4	HFR200-0.96/0.2	1117.6	19.97	1100.32	16.43
5	R 250	1147.6	11.66	1143.01	6.17
6	HFR250-0.68/0.2	1375.5	15.19	1336.8	8.12
7	HFR250-0.80/0.2	1300.2	14.12	1350.38	8.3
8	HFR250-0.96/0.2	1386.5	15.97	1486.68	9.46

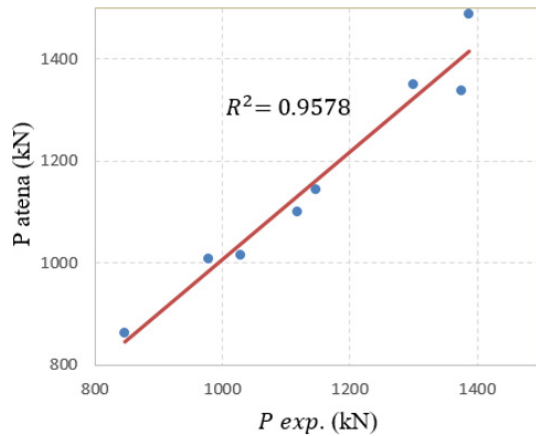


Fig. 8 Experimental results versus the FE analysis of load of slab models

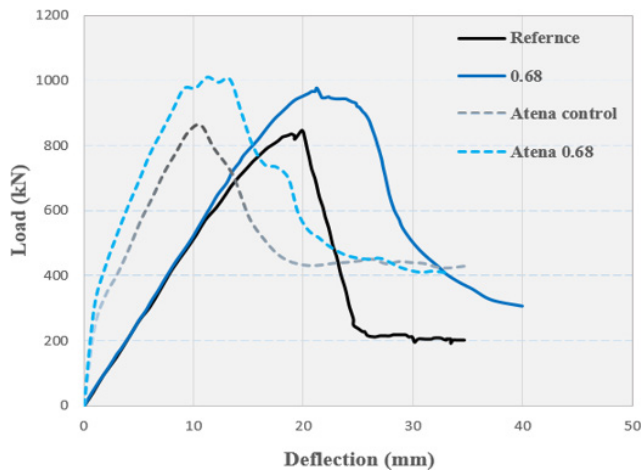


Fig. 9 The load-deflection curves of test and FE models for 200 mm thickness of reference and HFRC-0.68/0.2 slabs

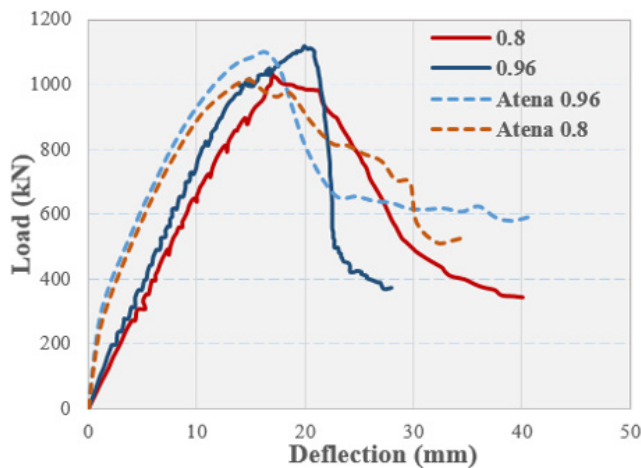


Fig. 10 The load-deflection curves of test and FE models for 200 mm thickness of HFRC-0.8/0.2 and HFRC-0.96/0.2 slabs

Table 7 presents the crack patterns observed in both the test specimens and the FE models of HFRC slabs, for both 200 mm and 250 mm thicknesses. It can be inferred that there is a reasonable agreement between them, facilitated

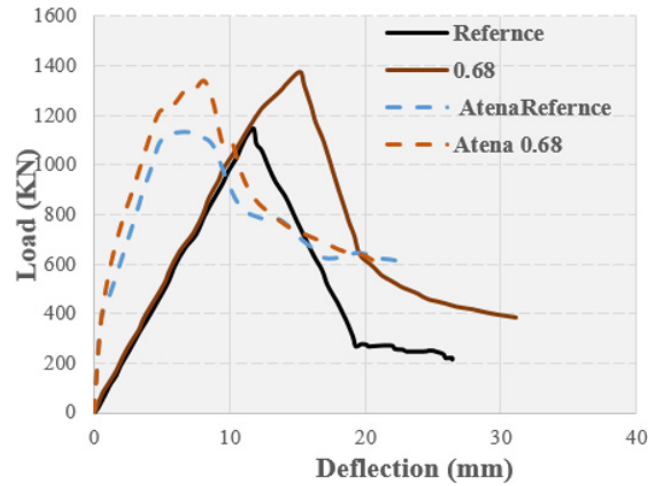


Fig. 11 The load-deflection curves of test and FE models for 250 mm thickness of reference and HFRC-0.68/0.2 slabs

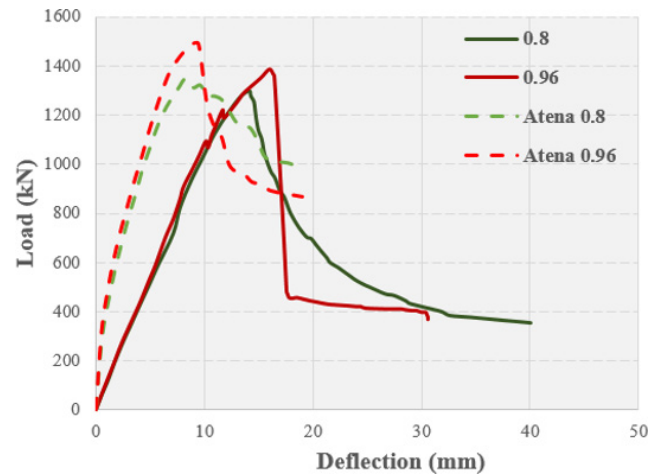


Fig. 12 The load-deflection curves of test and FE models for 250 mm thickness of HFRC-0.8/0.2 and HFRC-0.96/0.2 slabs

by the assumptions made in FE modeling. However, achieving crack patterns that precisely match experimental results may be challenging due to several factors. These include discrepancies between the assumptions of FE modeling and the actual behavior during loading tests, such as slippage of the reinforcement, variations in stiffness, and differences in failure criteria of the concrete under tension and compression [32–35].

3.2 FE modeling results and parametric study of HERC slabs

The ultimate loads-deflections of FE modeling slab results are presented in Tables 8 to 10. The designation of slabs in tables contains three terms, the first term is (HFRC) which represents the hybrid fiber reinforced concrete. The second term is (R) or (No./No.) which represents the control specimens for (R) symbol, and (No./No.) represents the SF

Table 7 Summarizes the experimental cracking pattern compared to the FE cracking pattern for HFRC slabs of 200 mm and 250 mm thicknesses


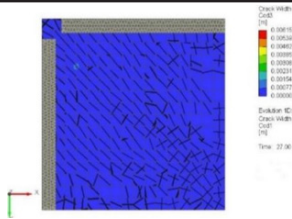

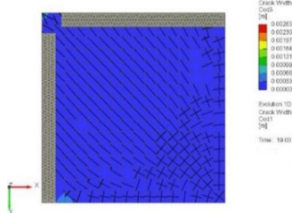

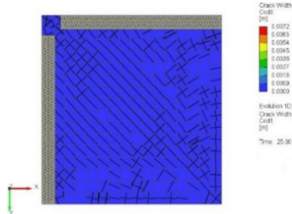
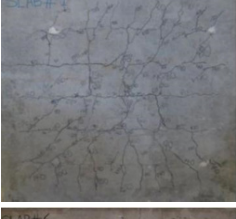
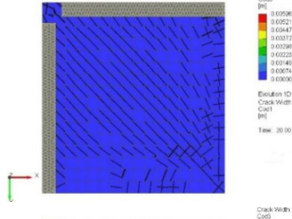

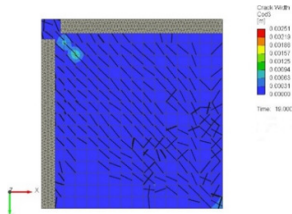
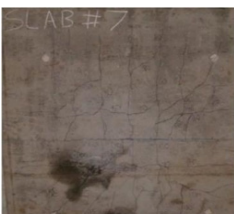
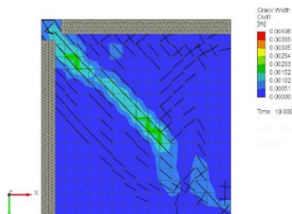

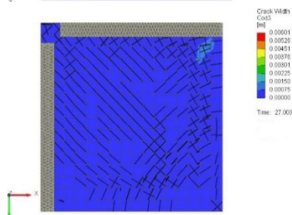
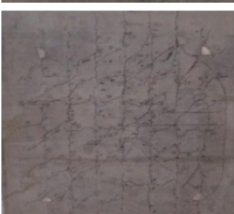
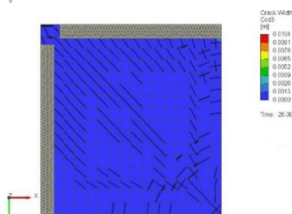
No.	Specimens name	Experimental cracks pattern	FE cracks pattern
1	R 200		
2	HFR200-0.68/0.2		
3	HFR200-0.80/0.2		
4	HFR200-0.96/0.2		
5	R 250		
6	HFR250-0.68/0.2		
7	HFR250-0.80/0.2		
8	HFR250-0.96/0.2		

Table 8 Displays the results of ultimate FE modelling loads when compressive strength (f'_c) = 50 MPa

No.	Specimens code	Steel reinforcement	f'_c (MPa)	Slab thickness (mm)	$\Delta_{ult.}$ (mm)	$P_{ult.}$ (kN)
1	HFRC-R-0.54	8Ø16@250	50	150	22.80	400.846
2	HFRC-R-0.84	8Ø20@250			17.83	473.172
3	HFRC-R-1.31	8Ø25@250			14.87	513.450
4	HFRC-0.68/0.2-0.54	8Ø16@250			17.87	527.762
5	HFRC-0.68/0.2-0.84	8Ø20@250			15.88	547.025
6	HFRC-0.68/0.2-1.31	8Ø25@250			14.88	586.775
7	HFRC-0.8/0.2-0.54	8Ø16@250			29.44	547.467
8	HFRC-0.8/0.2-0.84	8Ø20@250			19.95	557.170
9	HFRC-0.8/0.2-1.31	8Ø25@250			17.44	590.280
10	HFRC-0.96/0.2-0.54	8Ø16@250			24.68	563.682
11	HFRC-0.96/0.2-0.84	8Ø20@250	50	200	21.90	606.995
12	HFRC-0.96/0.2-1.31	8Ø25@250			14.89	623.778
13	HFRC-R-0.4	8Ø16@250			17.703	670.319
14	HFRC-R-0.63	8Ø20@250			15.009	819.776
15	HFRC-R-0.98	8Ø25@250			10.158	842.235
16	HFRC-0.68/0.2-0.4	8Ø16@250			19.38	875.657
17	HFRC-0.68/0.2-0.63	8Ø20@250			12.49	903.167
18	HFRC-0.68/0.2-0.98	8Ø25@250			9.86	872.899
19	HFRC-0.8/0.2-0.4	8Ø16@250			16.90	800.999
20	HFRC-0.8/0.2-0.63	8Ø20@250			12.00	833.803
21	HFRC-0.8/0.2-0.98	8Ø25@250	50	250	11.87	873.434
22	HFRC-0.96/0.2-0.4	8Ø16@250			19.52	862.374
23	HFRC-0.96/0.2-0.63	8Ø20@250			14.85	937.483
24	HFRC-0.96/0.2-0.98	8Ø25@250			11.90	963.232
25	HFRC-R-0.32	8Ø16@250			13.60	942.254
26	HFRC-R-0.5	8Ø20@250			11.86	1177.716
27	HFRC-R-0.79	8Ø25@250			7.94	1275.809
28	HFRC-0.68/0.2-0.32	8Ø16@250			10.11	1068.399
29	HFRC-0.68/0.2-0.5	8Ø20@250			7.96	1095.076
30	HFRC-0.68/0.2-0.79	8Ø25@250			7.83	1123.725
31	HFRC-0.8/0.2-0.32	8Ø16@250	50	250	11.11	1055.130
32	HFRC-0.8/0.2-0.5	8Ø20@250			11.52	1129.812
33	HFRC-0.8/0.2-0.79	8Ø25@250			10.26	1177.635
34	HFRC-0.96/0.2-0.32	8Ø16@250			15.75	1204.220
35	HFRC-0.96/0.2-0.5	8Ø20@250			10.57	1234.673
36	HFRC-0.96/0.2-0.79	8Ø25@250			6.70	1214.562

ratio for the first digit and synthetic fiber ratio for the second digit. The third term denotes the quantities of steel reinforcement ratio. To interpret tables, results, and the effect of each parameter on the punching shear capacity, consider the following points.

3.2.1 Influence of compressive strength (f'_c)

The compressive strength varied from 50, 70, and 90 MPa to investigate its effect on the punching shear capacity of

HFRC slabs. Based on the results of FE modeling in Tables 8 to 10, several Figs. 13 to 15 are constructed to simplify the role of compressive strength. Generally, it can be seen from Fig. 13 that the increase in the compressive strength leads to enhance in the shear capacity with different ratios of increment. However, for slabs with a thickness of 150 mm and a compressive strength of 90 MPa, significant increases in ultimate shear capacity are observed with different ratios of steel reinforcement and hybrid SF volume. Additionally,

Table 9 Displays the results of ultimate FE modelling loads when compressive strength (f'_c) = 70 MPa

No.	Specimens code	Steel reinforcement	f'_c (MPa)	Slab thickness (mm)	$\Delta_{ult.}$ (mm)	$P_{ult.}$ (kN)
1	HFRC-R-0.54	8Ø16@250	70	150	20.44	433.615
2	HFRC-R-0.84	8Ø20@250			17.52	486.880
3	HFRC-R-1.31	8Ø25@250			12.38	515.139
4	HFRC-0.68/0.2-0.54	8Ø16@250			20.1	621.518
5	HFRC-0.68/0.2-0.84	8Ø20@250			19.88	675.177
6	HFRC-0.68/0.2-1.31	8Ø25@250			17.38	720.778
7	HFRC-0.8/0.2-0.54	8Ø16@250			34.08	654.269
8	HFRC-0.8/0.2-0.84	8Ø20@250			27.94	709.913
9	HFRC-0.8/0.2-1.31	8Ø25@250			22.49	747.847
10	HFRC-0.96/0.2-0.54	8Ø16@250			27.39	670.869
11	HFRC-0.96/0.2-0.84	8Ø20@250			29.92	755.222
12	HFRC-0.96/0.2-1.31	8Ø25@250			14.88	725.589
13	HFRC-R-0.4	8Ø16@250	70	200	15.33	733.617
14	HFRC-R-0.63	8Ø20@250			14.97	859.187
15	HFRC-R-0.98	8Ø25@250			10.13	866.794
16	HFRC-0.68/0.2-0.4	8Ø16@250			23.88	1051.832
17	HFRC-0.68/0.2-0.63	8Ø20@250			16.89	1147.884
18	HFRC-0.68/0.2-0.98	8Ø25@250			13.87	1132.437
19	HFRC-0.8/0.2-0.4	8Ø16@250			23.12	941.995
20	HFRC-0.8/0.2-0.63	8Ø20@250			16.67	1077.884
21	HFRC-0.8/0.2-0.98	8Ø25@250			13.90	1137.842
22	HFRC-0.96/0.2-0.4	8Ø16@250			23.89	1048.467
23	HFRC-0.96/0.2-0.63	8Ø20@250			21.30	1160.079
24	HFRC-0.96/0.2-0.98	8Ø25@250			14.43	1215.781
25	HFRC-R-0.32	8Ø16@250	70	250	11.19	1057.787
26	HFRC-R-0.5	8Ø20@250			11.79	1233.948
27	HFRC-R-0.79	8Ø25@250			8.10	1261.012
28	HFRC-0.68/0.2-0.32	8Ø16@250			12.18	1278.152
29	HFRC-0.68/0.2-0.5	8Ø20@250			9.25	1368.050
30	HFRC-0.68/0.2-0.79	8Ø25@250			7.81	1350.150
31	HFRC-0.8/0.2-0.32	8Ø16@250			18.37	1320.526
32	HFRC-0.8/0.2-0.5	8Ø20@250			13.95	1429.661
33	HFRC-0.8/0.2-0.79	8Ø25@250			11.37	1487.188
34	HFRC-0.96/0.2-0.32	8Ø16@250			15.73	1382.240
35	HFRC-0.96/0.2-0.5	8Ø20@250			16.77	1602.163
36	HFRC-0.96/0.2-0.79	8Ø25@250			10.32	1641.007

Fig. 14 clearly depicts the notable enhancements in shear capacity as the slab thickness increases to 200 mm, particularly when the compressive strength is 70 MPa, in addition to 90 MPa. When the slab thickness equals 250 mm, the effective value of compressive strength is 70 MPa which can be observed in Fig. 15. It can be seen from Figs. 13 to 15 that there is no perfect role of fibers when slabs are thick 250 mm with 50 MPa compressive strength, the role of fibers be clear to participants to improve the shear capacity of slabs when the slabs are less than 250 mm with higher compressive

strength than 50 MPa. This result requires further evaluation to understand the behavior of compressive strength for other parameters, so a two-dimensional interaction drawing was drawn in Fig. 16. This interaction diagram presents a global assessment of the effects of various parameters on the shear capacity. The engineers can use this to design materials with the desired thickness, reinforcing, fiber content, and concrete strength that satisfy specific strength needs. The most evident result obtained out of the analysis is that the valid value of compressive strength is 90 MPa for a slab thickness

Table 10 Displays the results of ultimate FE modelling loads when compressive strength (f'_c) = 90 MPa

No.	Specimens code	Steel reinforcement	f'_c (MPa)	Slab thickness (mm)	$\Delta_{ult.}$ (mm)	$P_{ult.}$ (kN)
1	HFRC-R-0.54	8Ø16@250	90	150	20.02	441.870
2	HFRC-R-0.84	8Ø20@250			18.65	482.307
3	HFRC-R-1.31	8Ø25@250			13.18	526.632
4	HFRC-0.68/0.2-0.54	8Ø16@250			24.55	693.564
5	HFRC-0.68/0.2-0.84	8Ø20@250			21.87	767.156
6	HFRC-0.68/0.2-1.31	8Ø25@250			17.37	827.628
7	HFRC-0.8/0.2-0.54	8Ø16@250			29.88	725.723
8	HFRC-0.8/0.2-0.84	8Ø20@250			35.14	808.572
9	HFRC-0.8/0.2-1.31	8Ø25@250			24.96	889.733
10	HFRC-0.96/0.2-0.54	8Ø16@250			26.84	728.246
11	HFRC-0.96/0.2-0.84	8Ø20@250			29.89	846.166
12	HFRC-0.96/0.2-1.31	8Ø25@250			27.39	951.764
13	HFRC-R-0.4	8Ø16@250	90	200	18.29	743.885
14	HFRC-R-0.63	8Ø20@250			12.78	872.338
15	HFRC-R-0.98	8Ø25@250			10.05	941.338
16	HFRC-0.68/0.2-0.4	8Ø16@250			18.58	1084.975
17	HFRC-0.68/0.2-0.63	8Ø20@250			23.31	1298.463
18	HFRC-0.68/0.2-0.98	8Ø25@250			16.28	1371.668
19	HFRC-0.8/0.2-0.4	8Ø16@250			26.89	1073.978
20	HFRC-0.8/0.2-0.63	8Ø20@250			21.05	1217.423
21	HFRC-0.8/0.2-0.98	8Ø25@250			18.09	1329.352
22	HFRC-0.96/0.2-0.4	8Ø16@250			27.38	1104.602
23	HFRC-0.96/0.2-0.63	8Ø20@250			23.52	1298.605
24	HFRC-0.96/0.2-0.98	8Ø25@250			18.78	1450.582
25	HFRC-R-0.32	8Ø16@250	90	250	14.43	1140.609
26	HFRC-R-0.5	8Ø20@250			11.72	1373.926
27	HFRC-R-0.79	8Ø25@250			10.28	1626.605
28	HFRC-0.68/0.2-0.32	8Ø16@250			12.19	1351.901
29	HFRC-0.68/0.2-0.5	8Ø20@250			11.61	1581.310
30	HFRC-0.68/0.2-0.79	8Ø25@250			7.91	1625.040
31	HFRC-0.8/0.2-0.32	8Ø16@250			22.35	1533.329
32	HFRC-0.8/0.2-0.5	8Ø20@250			15.20	1657.840
33	HFRC-0.8/0.2-0.79	8Ø25@250			11.38	1688.899
34	HFRC-0.96/0.2-0.32	8Ø16@250			20.70	1527.296
35	HFRC-0.96/0.2-0.5	8Ø20@250			20.41	1843.305
36	HFRC-0.96/0.2-0.79	8Ø25@250			14.00	1945.267

of 150 mm, and the valid limit of steel-reinforced ratio is 0.54% for 70 and 90 MPa compressive strength. The hybrid SF behavior appears to suggest that the optimum ratio is 0.96% at a compressive strength of 50 MPa and 0.68% at a compressive strength of 90 MPa.

3.2.2 Influence of slab thickness (h)

In general, the relationship between slab thickness and punching shear capacity is inverse, indicating that as the

thickness of the slab increases, its susceptibility to punching decreases. but when some parameters were entered into the slab design, the principle of slab thickness would be different. However, it can be concluded from the results of modeling and statistical analysis in Fig. 16 that the effective thickness of slab is equal to 150 mm when the compressive strength is variable from 50, 70, and 90 MPa, besides the effective ratio of hybrid SF which is equal to 0.96% with a perfect ratio of 0.54% of steel reinforcement.

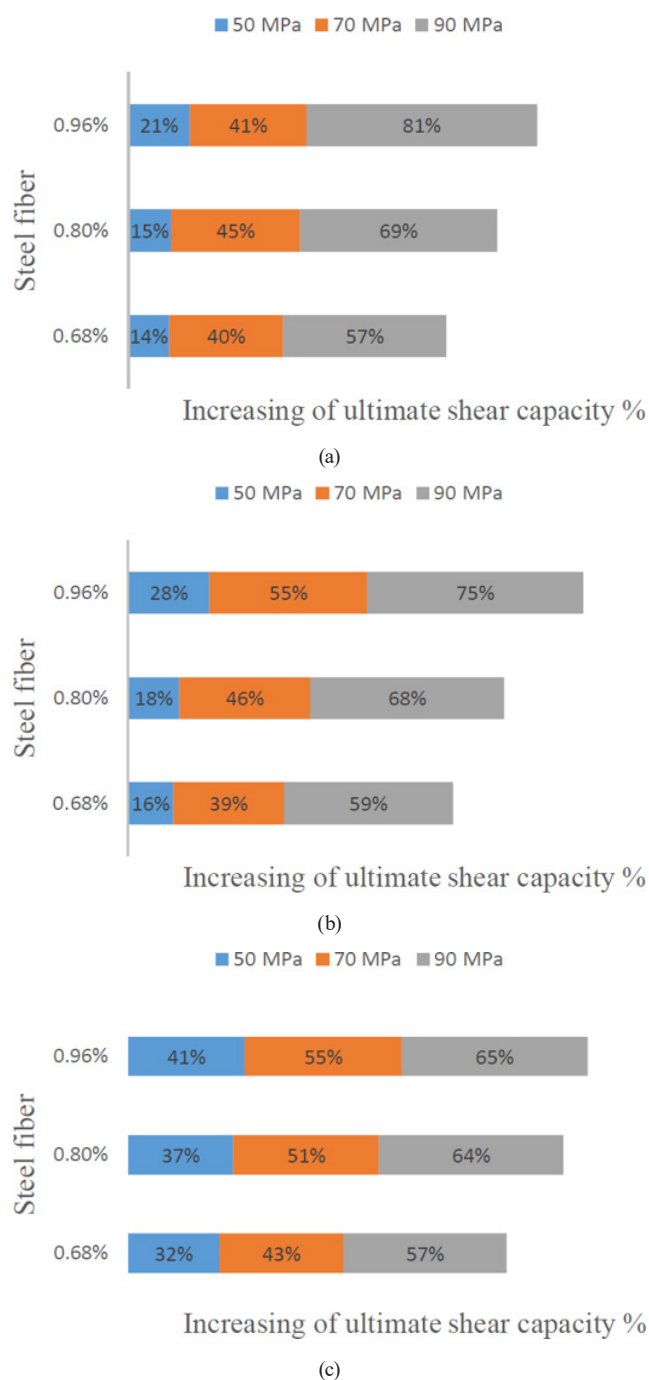


Fig. 13 The effect of compressive strength on the punching shear capacity of HFRC slabs with thickness 150 mm at (a) $\rho = 1.31\%$, (b) $\rho = 0.84\%$, (c) $\rho = 0.54\%$

These findings indicate that the effective ratio of hybrid SF contributes to decreasing the effective thickness of slab and steel reinforcement ratio which gives significant results of punching shear strength.

3.2.3 Influence of steel reinforcement ratio (ρ)

In this study, three diameters of main steel reinforcement are utilized: 16 mm, 20 mm, and 25 mm, corresponding

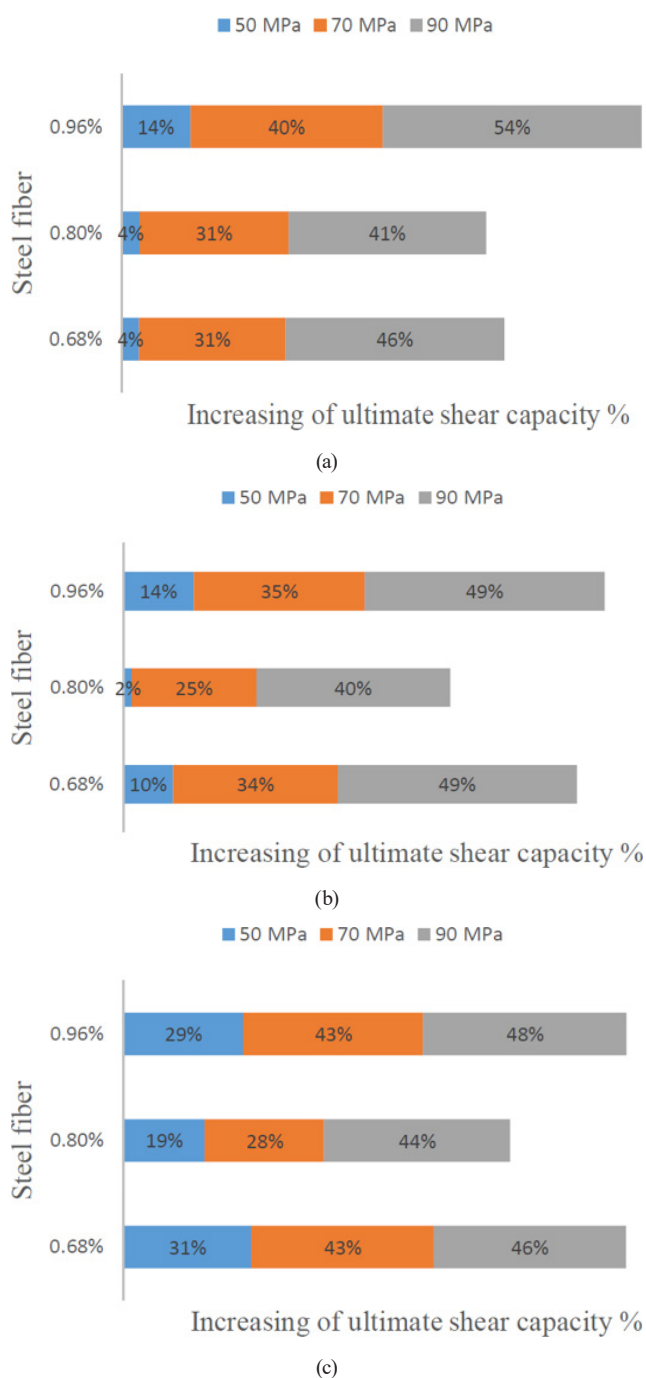


Fig. 14 The effect of compressive strength on the punching shear capacity of HFRC slabs with thickness 200 mm at (a) $\rho = 0.98\%$, (b) $\rho = 0.63\%$, (c) $\rho = 0.4\%$

to steel reinforcement ratios of 0.54%, 0.84%, and 1.31% for a slab thickness of 150 mm. Similarly, ratios of 0.40%, 0.63%, and 0.98% are employed for a slab thickness of 200 mm, and ratios of 0.32%, 0.5%, and 0.79% are utilized for a slab thickness of 250 mm.

The findings of this study suggest that the most effective ratio of steel reinforcement is 0.54% when the compressive strength varies from 50 MPa to 90 MPa. Furthermore, this

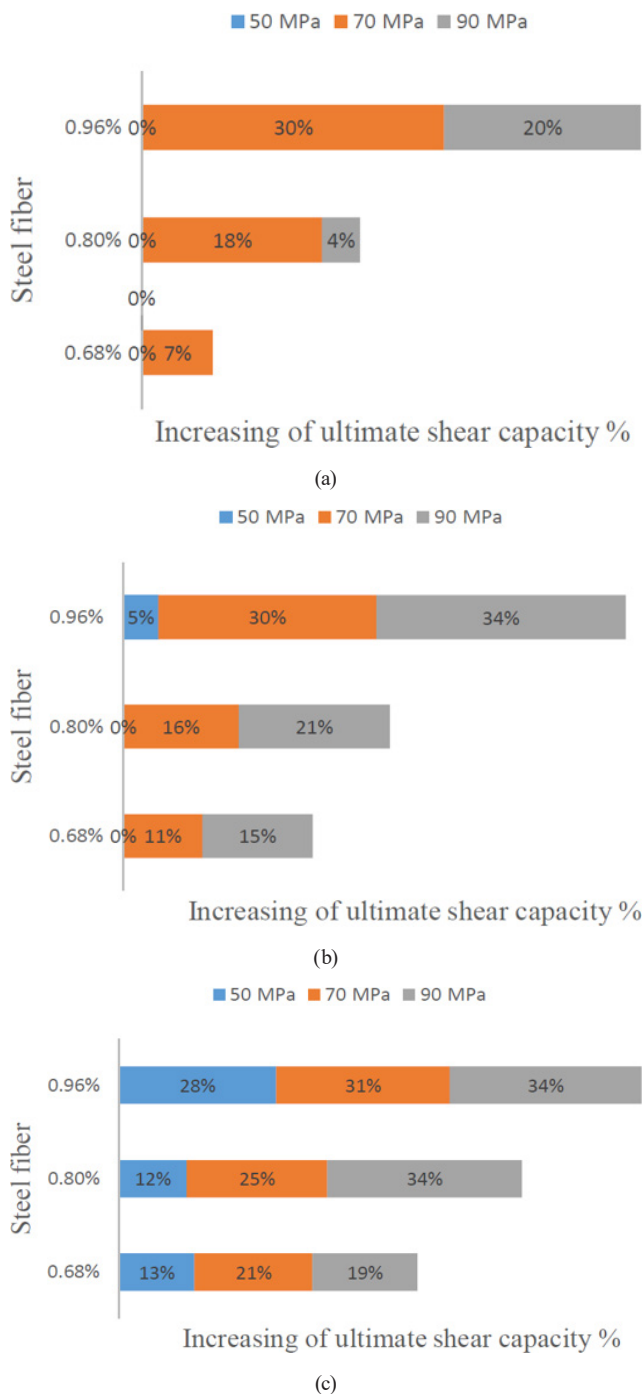


Fig. 15 The effect of compressive strength on the punching shear capacity of HFRC slabs with thickness 250 mm at (a) $\rho = 0.79\%$, (b) $\rho = 0.5\%$, (c) $\rho = 0.32\%$

0.54% ratio yields superior results when the slab thickness is 150 mm and the hybrid SF ratio is 0.96%.

3.2.4 Influence of hybrid SF ratio (V_f)

Two types of fibers were used together in this research: SF and macro synthetic fibers. SF has three volumetric ratios; of 0.68%, 0.8%, and 0.96%. Besides, the macro synthetic fibers 0.2% for all specimens.

Figs. 17 to 19 show the interpretation of results in Tables 8 to 10. It can be seen the increase in the ultimate shear capacity *via* hybrid SF ratios. Moreover, when using 0.96% of a hybrid SF ratio, the ultimate shear capacity was perfectly improved with a slab thickness of 150 mm and 90 MPa of compressive strength. This conclusion can be easily seen in Fig. 17 which represents more economic and optimistic results concerning the ultimate shear capacity. However, there is no improvement in the shear capacity *via* hybrid fibers when the thickness of the slab is 250 mm, the compressive strength is 50 MPa, and the main steel reinforcement ratios are greater than or equal to 0.5% as shown in Figs. 18 and 19. This might be related to the size effect on the normal punching shear strength which is a more significant effect than other variables [20, 36–38].

Fig. 20 illustrates the effectiveness of each parameter in determining the ultimate shear capacity. It is evident that each parameter significantly influences the shear capacity. Furthermore, the combinations of parameters that yield the most attractive values of ultimate shear strength are as follows: compressive strength (f'_c) of 90 MPa, slab thickness (h) of 150 mm, steel reinforcement ratio of 0.54%, and SF ratio of 0.96%.

These results support the idea that increasing the compressive strength makes the shear capacity better. However, the improvement is bigger when the compressive strength ranges from 50 MPa to 70 MPa than when it ranges from 70 MPa to 90 MPa. Therefore, the designer should prioritize 70 MPa over 90 MPa for a more cost-effective and efficient compressive strength value. Additionally, a slab thickness of 150 mm, a steel reinforcement ratio of 0.54%, and a SF ratio of 0.96% are recommended for achieving optimal shear capacity.

4 Conclusions

The present study was designed to determine the effect of hybrid SF ratios on the shear capacity of a flat slab (1900 × 1900 mm) when the depth of the slab thickness (h), steel reinforcement ratio, and compressive strength are set variables. Three groups of slab models were created to analyze the effect of different values of high compressive strength (f'_c) of 50, 70, and 90 MPa, slab thickness (h mm) of 150, 200, and 250 mm, and different steel reinforcement ratios based on 3 types of main steel bars reinforcement 16, 20, and 25 mm in diameter, as well as a different ratio of hybrid SF reinforcement, consisting of 0.68, 0.8, and 0.96 % of SF with 0.2% of macro synthetic fibers. The total slab models equal 108 models constructed from three groups. Moreover, 8 slab models were used to

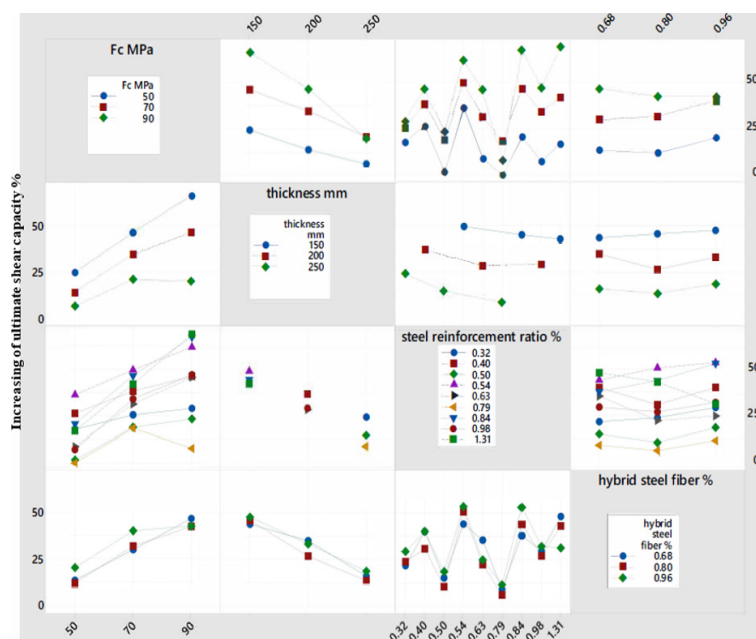


Fig. 16 2D interaction plot of ultimate shear capacity concerning the parameters (compressive strength (f'_c), slab thickness (h), steel reinforcement ratios (%), and hybrid SF ratios (%))

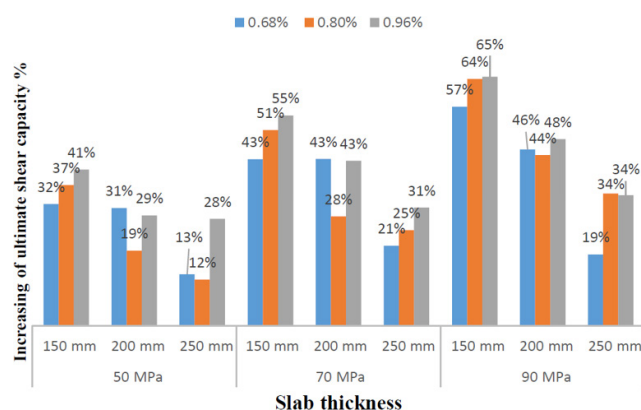


Fig. 17 Influence of hybrid SF ratio on the punching shear capacity of HFRc slabs at all slab thickness and compressive strength with steel bar 16 mm

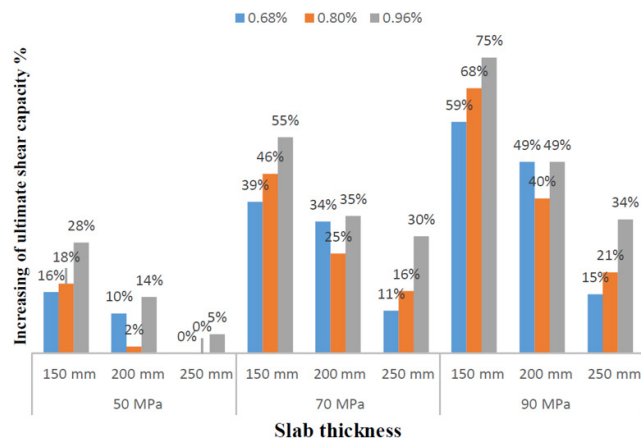


Fig. 18 Influence of hybrid SF ratio on the punching shear capacity of HFRc slabs at all slab thickness and compressive strength with steel bar 20 mm

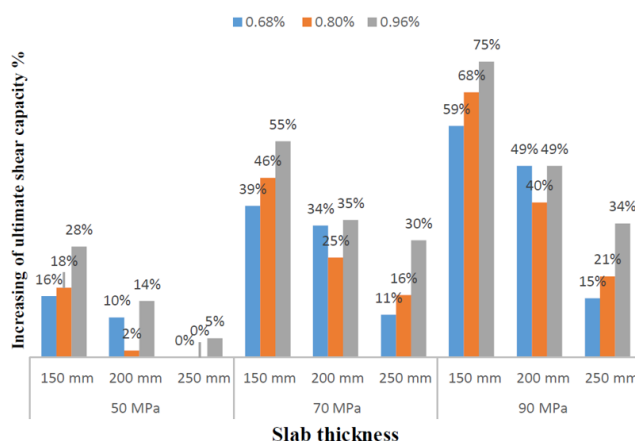


Fig. 19 Influence of hybrid SF ratio effect on the punching shear capacity of HFRc slabs at all slab thickness and compressive strength with steel bar 25 mm

verify the materials of FE modeling. This study of modeling punching flat slabs identified the following points:

- The verification materials of FE modelling analysis tend to be accurate with the experimental results with a correlation coefficient $R^2 = 0.9578$. However, major differences exist between the FE analysis and the experimental test results for the displacement. These differences might happen because the FE model makes too many simple assumptions, such as the steel reinforcement and concrete always sticking together perfectly. These assumptions do not fully reflect the reality of experimental tests.

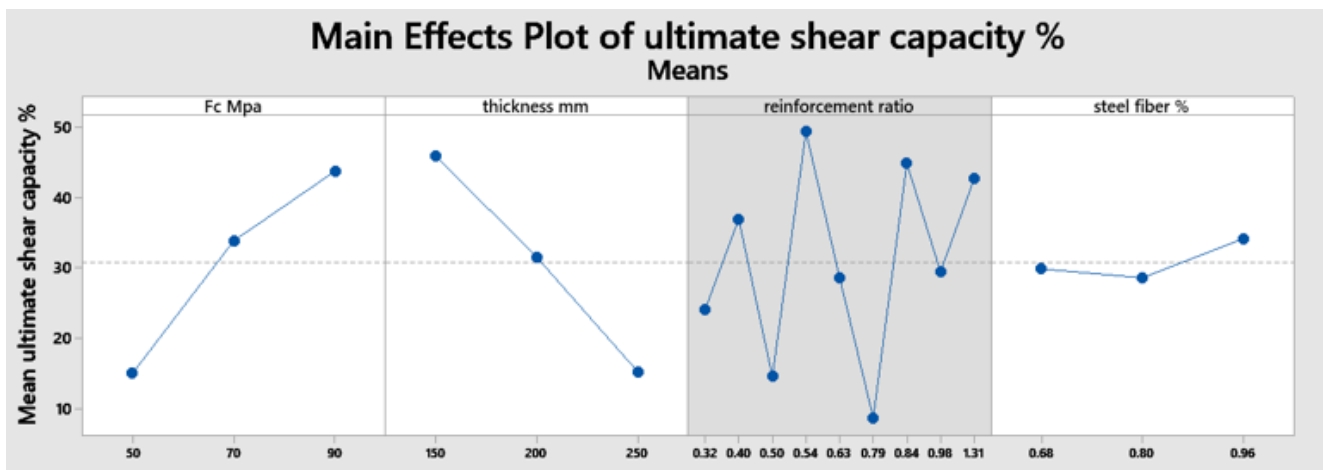


Fig. 20 Main effects graphs of ultimate shear capacity concerning the parameters of the study

- The ultimate shear capacity improved with different ratios of hybrid SF addition.
- In general, when increasing the design thickness of the slab, shear strength capacity will be increased and punching failure will be decreased. But when using hybrid SF additive, the conception of increasing thickness will be different.
- The findings of this study set out to explore the influence of hybrid SF additives which are suggested to use 0.96% of SF with 0.2% macro synthetic fibers to decrease the thickness of the slab from 250 mm to 150 mm to give a better result against punching shear failure.
- The application of high compressive strength in flat slabs contributes to an enhancement in their shear capacity. However, when the compressive strength varies from 50 MPa to 70 MPa and 90 MPa, significant improvements are observed, with a more notable average improvement noted when increasing the compressive strength from 50 MPa to 70 MPa.
- Employing an optimal ratio of hybrid SF resulted in a reduction in the quantity of steel reinforcement, specifically at 0.54%, when using 16 mm main bar reinforcement with a thickness of $h = 150$ mm. This ratio significantly enhances the shear capacity, mitigating the risk of punching failure in flat slabs. The present findings might help the designer to calculate the ideal economic ratio of hybrid SF, steel reinforcement, compressive strength value as well as the ideal thickness of the flat slab. However, the findings show that when using compressive strength 90 MPa, 0.96% of SF besides 0.2% of macro synthetic fibers, slab thickness 150 mm, and 0.54% of steel reinforcement ratio, shear capacity was significantly improved with decreasing in punching shear failure capability of flat slab.

References

- [1] Al-Ta'an, S. A., Abdul-Razzak, A. A. "Geometrical and Material Nonlinear Finite Analysis of Fiber Reinforced Concrete Slabs", IOP Conference Series: Materials Science and Engineering, 978(1), 012041, 2020.
<https://doi.org/10.1088/1757-899X/978/1/012041>
- [2] Barros, J. A. O., Moraes Neto, B. N., Melo, G. S. S. A., Frazão, C. M. V. "Assessment of the effectiveness of steel fibre reinforcement for the punching resistance of flat slabs by experimental research and design approach", Composites Part B: Engineering, 78, pp. 8–25, 2015.
<https://doi.org/10.1016/j.compositesb.2015.03.050>
- [3] Mabrouk, R. T. S., Hegab, A. A. "Analysis of the punching behavior of RC flat slabs with horizontal and vertical shear reinforcement", MATEC Web of Conferences, 120, 01006, 2017.
<https://doi.org/10.1051/mateconf/201712001006>
- [4] Haryanto, Y., Hu, H.-T., Han, A. L., Hsiao, F.-P., Teng, C.-J., Hidayat, B. A., Nugroho, L. "Nonlinear 3D Model of Double Shear Lap Tests for the Bond of Bear-surface Mounted FRP Rods in Concrete Considering Different Embedment Depth", Periodica Polytechnica Civil Engineering, 65(3), pp. 878–889, 2021.
<https://doi.org/10.3311/PPci.17309>
- [5] Aziz, A. H., Kareem, S. S., Sahib A., B. "Experimental Study for Punching Shear Behavior in RC Flat Plate with Hybrid High Strength Concrete", Journal of Engineering and Sustainable Development, 17(3), pp. 105–119, 2013. [online] Available at: <https://jeasd.uomustansiriyah.edu.iq/index.php/jeasd/article/view/1001> [Accessed: 20 June 2024]

- [6] Koppitz, R., Kenel, A., Keller, T. "Punching shear of RC flat slabs – Review of analytical models for new and strengthening of existing slabs", *Engineering Structures*, 52, pp. 123–130, 2013.
<https://doi.org/10.1016/j.engstruct.2013.02.014>
- [7] AL-Eliwi, B. J., Sheet, N. M., Najem, R. M., Hasan, W. M. "The Optimum Design of RC Beams Strengthened with FRP Materials: A Review", *Al-Rafidain Engineering Journal (AREJ)*, 28(2), pp. 18–32, 2023.
<https://doi.org/10.33899/rengj.2023.139008.1244>
- [8] Labib, W. A. "Evaluation of hybrid fibre-reinforced concrete slabs in terms of punching shear", *Construction and Building Materials*, 260, 119763, 2020.
<https://doi.org/10.1016/j.conbuildmat.2020.119763>
- [9] Almusallam, T. H., Abadel, A. A., Al-Salloum, Y. A., Siddiqui, N. A., Abbas, H. "Effectiveness of hybrid-fibers in improving the impact resistance of RC slabs", *International Journal of Impact Engineering*, 81, pp. 61–73, 2015.
<https://doi.org/10.1016/j.ijimpeng.2015.03.010>
- [10] Mohammad, S. H., Gülşan, M. E., Çevik, A. "A Detailed Investigation of the Bond Performance of Basalt Fiber-Reinforced Polymer Bars in Geopolymer Concrete", *Periodica Polytechnica Civil Engineering*, 66(2), pp. 471–490, 2022.
<https://doi.org/10.3311/PPci.18997>
- [11] Kobayashi, K., Cho, R. "Flexural characteristics of steel fibre and polyethylene fibre hybrid-reinforced concrete", *Composites*, 13(2), pp. 164–168, 1982.
[https://doi.org/10.1016/0010-4361\(82\)90054-4](https://doi.org/10.1016/0010-4361(82)90054-4)
- [12] Sermet, F., Ozdemir, A. "Investigation of Punching Behaviour of Steel and Polypropylene Fibre Reinforced Concrete Slabs under Normal Load", *Procedia Engineering*, 161, pp. 458–465, 2016.
<https://doi.org/10.1016/j.proeng.2016.08.590>
- [13] ACI Committee 544 "Guide for Specifying, Proportioning, Mixing, Placing, and finishing steel Fiber Reinforced Concrete", *ACI Materials Journal*, 90(1), pp. 94–103, 1993.
<https://doi.org/10.14359/4046>
- [14] Pujadas, P., Blanco-Alvarez, A., Pialarissi-Cavalero, S., De la Fuente, A., Aguado, A. "Flat suspended slabs reinforced only with macro-synthetic fibres", *Loughborough University*, 2016. [online] Available at: <https://hdl.handle.net/2134/32379> [Accessed: 20 June 2024]
- [15] Shoaib, A., Lubell, A. S., Bindiganavile, V. S. "Size Effect in Shear for Steel Fiber-Reinforced Concrete Members without Stirrups", *ACI Structural Journal*, 111(5), pp. 1081–1090, 2014.
<https://doi.org/10.14359/51686813>
- [16] ACI Committee 544 "State-of-the-Art Report on Fiber Reinforced Concrete", *ACI Committee*, Detroit, MI, USA, Rep. ACI 544.1R-96, 1996.
- [17] Kinnunen, S., Nylander, H. "Punching of concrete slabs without shear reinforcement", *Elander*, New York, NY, USA, 1960.
- [18] Haghgoo, M., Bahar, A. "Adhesive Layer Modeling in Concrete Beam Strengthened with FRP in an EFG Framework", *Periodica Polytechnica Civil Engineering*, 66(3), pp. 720–730, 2022.
<https://doi.org/10.3311/PPci.19654>
- [19] Bazant, Z. P., Cao, Z. "Size Effect in Punching Shear Failure of Slabs", *ACI Structural Journal*, 84(1), pp. 44–53, 1987.
<https://doi.org/10.14359/2785>
- [20] Caratelli, A., Imperatore, S., Meda, A., Rinaldi, Z. "Punching shear behavior of lightweight fiber reinforced concrete slabs", *Composites Part B: Engineering*, 99, pp. 257–265, 2016.
<https://doi.org/10.1016/j.compositesb.2016.06.045>
- [21] Pourreza, R. "Investigating the effects of hybrid fibres on the structural behaviour of two-way slabs", *MSc Thesis*, Memorial University of Newfoundland, 2014. [online] Available at: <http://research.library.mun.ca/id/eprint/6308> [Accessed: 20 June 2024]
- [22] Abbass, W., Khan, M. I., Mourad, S. "Evaluation of mechanical properties of steel fiber reinforced concrete with different strengths of concrete", *Construction and Building Materials*, 168, pp. 556–569, 2018.
<https://doi.org/10.1016/j.conbuildmat.2018.02.164>
- [23] Tan, K. H., Venkateshwaran, A. "Punching Shear in Steel Fibre Reinforced Concrete Slabs Without Traditional Reinforcement", *IOP Conference Series: Materials Science and Engineering*, 246(1), 012025, 2017.
<https://doi.org/10.1088/1757-899X/246/1/012025>
- [24] AlHamaydeh, M., Anwar Orabi, M. "Punching Shear Behavior of Synthetic Fiber-Reinforced Self-Consolidating Concrete Flat Slabs with GFRP Bars", *Journal of Composites for Construction*, 25(4), 04021029, 2021.
[https://doi.org/10.1061/\(ASCE\)CC.1943-5614.0001131](https://doi.org/10.1061/(ASCE)CC.1943-5614.0001131)
- [25] Khan, Q. u. Z., Ali, M., Ahmad, A., Raza, A., Iqbal, M. "Experimental and finite element analysis of hybrid fiber reinforced concrete two-way slabs at ultimate limit state", *SN Applied Sciences*, 3(1), 73, 2021.
<https://doi.org/10.1007/s42452-020-04078-y>
- [26] Červenka Consulting "ATENA-GiD, (5.3)", [computer program] Available at: <https://www.cervenka.cz/download/> [Accessed: 25 February 2025]
- [27] Červenka, V., Červenka, J., Janda, Z., Pryl, D. "ATENA Program Documentation: Part 8: User's Manual for ATENA-GiD Interface", [pdf] Červenka Consulting s.r.o., Prague, Czech Republic, 2021. Available at: https://www.cervenka.cz/assets/files/atena-pdf/ATENA-Science-GiD_Users_Manual.pdf [Accessed: 03 March 2025]
- [28] Menetrey, P., Willam, K. J. "Triaxial Failure Criterion for Concrete and its Generalization", *ACI Structural Journal*, 92(3), pp. 311–318, 1995.
<https://doi.org/10.14359/1132>
- [29] Červenka, V., Jendele, L., Červenka, J. "ATENA Program Documentation: Part 1: Theory!", [pdf] Červenka Consulting s.r.o., Prague, Czech Republic, 2018. Available at: <https://www.scribd.com/document/425359412/ATENA-Theory-1-pdf> [Accessed: 03 March 2025]
- [30] Sajdlová, T. "ATENA Program Documentation: Part 4-7: ATENA Science – GiD FRC Tutorial: Step by step guide for nonlinear analysis of fiber reinforced concrete structures with ATENA and GiD", [pdf] Červenka Consulting s.r.o., Prague, Czech Republic, 2016. Available at: https://www.cervenka.cz/assets/files/atena-pdf/ATENA-Science-GiD_Tutorial_FRC.pdf [Accessed: 03 March 2025]
- [31] Nghiep, V. H. "Shear design of straight and haunched concrete beams without stirrups", *PhD Thesis*, Technische Universität Hamburg, 2011.
<https://doi.org/10.15480/882.1050>

- [32] Al Jawahery, M. S., Gulsan, M. E., Albegmprli, H. M., Mansoori, I. A. H., Cevik, A. "Experimental investigation of rehabilitated RC haunched beams via CFRP with 3D-FE modeling analysis", *Engineering Structures*, 196, 109301, 2019.
<https://doi.org/10.1016/j.engstruct.2019.109301>
- [33] Al Jawahery, M. S., Gülşan, M. E., Albegmprli, H. M. A., Çevik, A. "Comprehensive Shear and Flexural Study: Experimental and FE Modeling of RC Haunched Beams Rehabilitated by Basalt Fabric", *Iranian Journal of Science and Technology, Transactions of Civil Engineering*, 46(3), pp. 1887–1914, 2022.
<https://doi.org/10.1007/s40996-021-00741-5>
- [34] Al Jawahery, M. S., Çevik, A., Gülşan, M. E. "3D FE modeling and parametric analysis of steel fiber reinforced concrete haunched beams", *Advances in Concrete Construction*, 13(1), pp. 45–69, 2022.
<https://doi.org/10.12989/acc.2022.13.1.045>
- [35] AL-Eliwi, B. J. M., Al Jawahery, M. S. "Numerical analysis for the punching shear resistance of SFRC flat slabs", *Computers and Concrete*, 32(4), pp. 425–438, 2023.
<https://doi.org/10.12989/cac.2023.32.4.425>
- [36] Birkle, G., Dilger, W. H. "Influence of slab thickness on punching shear strength", *ACI Structural Journal*, 105(2), pp. 180–188, 2008. [online] Available at: <https://www.proquest.com/openview/7c9de11cb7a1316226648553a36e7168/1?pq-origsite=gscholar&cbl=36963> [Accessed: 20 June 2024]
- [37] Navarro, M., Ivorra, S., Varona, F. B. "Parametric computational analysis for punching shear in RC slabs", *Engineering Structures*, 165, pp. 254–263, 2018.
<https://doi.org/10.1016/j.engstruct.2018.03.035>
- [38] Iravani, S. "Mechanical Properties of High-Performance Concrete", *ACI Materials Journal*, 93(5), pp. 416–426, 1996.
<https://doi.org/10.14359/9845>

Appendix A

This part presents the concrete material properties of HFRC with volume fractions of fibers, besides the mathematical relations for calculating the tensile function and fiber tensile strength. Tables A1 to A4 show the concrete material properties used in the FE analysis.

In the case of all the ATENA concrete fiber models, the tensile function that gives the relationship between tensile stress and strain is derived from results related to four-point bending tests in order to evaluate the tensile strength. The tensile function in the model illustrates the relationship between fracture strain (horizontal axis) and

Table A1 Concrete material properties used in FE modeling with 0% fibers

Structural element	Unit		Reference 0%		
Compressive strength	f'_c	MPa	50	70	90
Material prototype	–	–	CC3D non-linear Cementitious2 [29]	CC3D non-linear Cementitious2 [29]	CC3D non-linear Cementitious2 [29]
Elastic modulus	E_c	MPa	26870.1	31793.08	36049.9
Poisson's ratio	μ	–	0.2	0.2	0.2
Tensile strength	f_t	MPa	3.62	4.41	4.88

Table A2 Concrete material properties used in FE modelling with 0.68% SFs and 0.2% synthetic fibers

Structural element	Unit		0.68%, 0.2%		
Compressive strength	f'_c	MPa	50	70	90
Material prototype	–	–	CC3D non-linear Cementitious2 user [29]	CC3D non-linear Cementitious2 user [29]	CC3D non-linear Cementitious2 user [29]
Elastic modulus	E_c	MPa	28306.5	33492.6	37977.08
Poisson's ratio	μ	–	0.2	0.2	0.2
Tensile strength	f_t	MPa	9.56	12.96	15.84

Table A3 Concrete material properties used in FE modelling with 0.80% SFs and 0.2% synthetic fibers

Structural element	Unit		0.80%, 0.2%		
Compressive strength	f'_c	MPa	50	70	90
Material prototype	–	–	CC3D non-linear Cementitious2 user [29]	CC3D non-linear Cementitious2 user [29]	CC3D non-linear Cementitious2 user [29]
Elastic modulus	E_c	MPa	28557.5	33789.6	38313.87
Poisson's ratio	μ	–	0.2	0.2	0.2
Tensile strength	f_t	MPa	9.59	12.99	15.86

Table A4 Concrete material properties used in FE modelling with 0.68% SFs and 0.2% synthetic fibers

Structural element	Unit	0.96%, 0.2%		
Compressive strength f'_c	MPa	50	70	90
Material prototype	–	CC3D non-linear Cementitious2 user [29]	CC3D non-linear Cementitious2 user [29]	CC3D non-linear Cementitious2 user [29]
Elastic modulus	E_c	28896.8	34191.1	38769.1
Poisson's ratio	μ	0.2	0.2	0.2
Tensile strength	f_t	9.63	13.03	15.89

the ratio of tensile stress to tensile strength (vertical axis). Fig. A1 illustrates the tensile properties of HFRC.

The fracture strain is calculated using Eq. (A1) [30]:

$$\varepsilon_f = w_c / L_t, \quad (\text{A1})$$

where:

- ε_f : fracture strain,
- w_c : crack opening,
- L_t : characteristic length.

More details are available in the ATENA Program Documentation [29]. Additional characteristics for the selected fiber type must be established to model punching shear for HFRC. Due to the absence of a predefined list of alternative fiber types in ATENA, the user must manually pick the material parameters to ensure they are sufficiently equivalent to the desired fiber type [29, 30]. It can be predicted the modulus of elasticity of concrete by using Eq. (A2), and besides the modulus of elasticity with fiber, it can be used Eq. (A3) [22, 38]. In addition to that, Eq. (A4)

may be utilized to calculate the fiber's reinforcing index, and Eq. (A5) can be used to estimate fiber tensile strength [22]:

$$E_c = 3.8 \sqrt{f'_c} \text{ for } 50 \text{ MPa} < f'_c < 125 \text{ MPa}, \quad (\text{A2})$$

$$E_{cf} = E_c [1 + 0.173(RI)], \quad (\text{A3})$$

$$RI = V_f \times L_f / \phi_f, \quad (\text{A4})$$

$$f_t = 0.15 f'_{cu} (1 - V_f) + 0.79 RI, \quad (\text{A5})$$

where:

- E_c : modulus of elasticity of plain concrete,
- L_f : fiber length,
- f'_c : compressive strength of plain concrete,
- ϕ_f : diameter of the fiber,
- E_{cf} : modulus of elasticity with fibers,
- f'_{cu} : cube compressive strength of concrete,
- RI : fiber's reinforcing index,
- f_t : fiber tensile strength,
- V_f : fiber volume fraction.

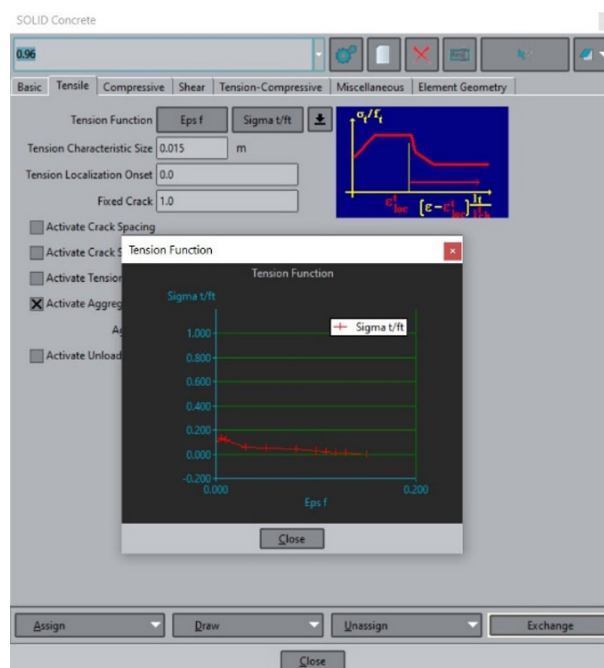


Fig. A1 FE tensile function of HFRC models